

Improved efficacy of a novel anti-angiogenic drug combination (TL-118) against colorectal-cancer liver metastases; MRI monitoring in mice

Y Edrei^{1,2,4}, E Gross^{3,4}, N Corchia¹ and R Abramovitch^{*,1,2}

¹Goldyne Savad Institute of Gene Therapy, Hadassah Hebrew University Medical Center, POB 12000, Jerusalem 91120, Israel; ²MRI/MRS lab HBRC, Hadassah Hebrew University Medical Center, Jerusalem 91120, Israel; ³Department of Pediatric Surgery, Hadassah Hebrew University Medical Center, Jerusalem 91120, Israel

BACKGROUND: The poor prognosis of patients with colorectal-cancer liver metastases (CRLM) and the insufficiency of available treatments have raised the need for alternative curative strategies. We aimed to assess the therapeutic potential of TL-118, a new anti-angiogenic drug combination, for CRLM treatment, in a mouse model.

METHODS: The therapeutic potential of TL-118 was evaluated and compared with B20-4.1.1 (B20; anti-VEGF antibody) and rapamycin in CRLM-bearing mice. Tumour progression and the vascular changes were monitored by MRI. Additionally, mice survival, cell proliferation, apoptosis and vessel density were evaluated.

RESULTS: This study demonstrated an unequivocal advantage to TL-118 therapy by significantly prolonging survival (threefold) and reducing metastasis perfusion and vessel density (ninefold). The underlying mechanism for TL-118-treatment success was associated with hepatic perfusion attenuation resulting from reduced nitric-oxide (NO) serum levels as elucidated by using hemodynamic response imaging (HRI, a functional MRI combined with hypercapnia and hyperoxia). Further, systemic hepatic perfusion reduction during the initial treatment phase by adding NO inhibitor has proven to be essential for reaching maximal therapeutic effects for both TL-118 and B20.

CONCLUSION: TL-118 harbours a potential clinical benefit to CLRM patients. Moreover, the reduction of hepatic perfusion at early stages of anti-angiogenic therapies by adding NO inhibitor is crucial for achieving maximal anti-tumour effects.

British Journal of Cancer (2012) **107**, 658–666. doi:10.1038/bjc.2012.322 www.bjcancer.com

Published online 17 July 2012

© 2012 Cancer Research UK

Keywords: hemodynamic response imaging; hyperoxia; hypercapnia; bevacizumab; liver perfusion

Colorectal cancer is the third most common cancer in the United States (Siegel *et al*, 2012), where colorectal-cancer liver metastases (CRLM) are the main cause of mortality among patients presenting advanced stages of the disease (McLoughlin *et al*, 2006). Despite improvements in surgical techniques and developments of new treatments, the prognosis of patients diagnosed with CRLM is still poor.

Angiogenesis is essential for solid tumour growth (Folkman, 1990) and critical to the metastatic cascade of CRLM development (Meyers and Watson, 2003). Therefore, anti-angiogenic therapy may offer an additional treatment option for this highly aggressive cancer (Warren *et al*, 1995; Meyers and Watson, 2003). Recently, several new anti-angiogenic agents have become available for advanced colorectal cancer treatment, but have failed to induce enduring clinical responses (Miller *et al*, 2005; Bergers and Hanahan, 2008). TL-118 is a novel drug combination that takes advantage of the multi-faceted nature of the angiogenic process; thus, it is composed of four agents that complement each other in their anti-angiogenic effect. In essence, each drug in this composition is aimed at a different aspect of the angiogenic

process: (i) Low-dose high-frequency cyclophosphamide, which drives tumour endothelial cell apoptosis as was shown by Browder *et al* (2000), (ii) The non-steroidal anti-inflammatory drug – diclofenac, which targets inflammatory cells, monocytes in particular, which has a pivotal role in early stages of angiogenesis (Grunewald *et al*, 2006; Mayorek *et al*, 2010), (iii) Sulfasalazin is an NF-kappaB inhibitor (Weber *et al*, 2000) that inhibit angiogenesis (Li *et al*, 2009), probably via vascular smooth muscle cell inhibition (Chung *et al*, 2009) and (iv) Cimetidine, a histamine type 2 (H2)-receptor blocker, demonstrated an anti-angiogenic activity probably via the inhibition of downstream targets of mast cells, which are known to have a role in the angiogenic process (Sorbo *et al*, 1994; Natori *et al*, 2005; Kubecova *et al*, 2011). This final composition was selected based on a systematic screening of multiple candidate agents. Those drugs that enhanced each other's anti-angiogenic activity in a tumour-bearing mouse model were further optimised with respect to their relative dose. All TL-118 components are approved drugs, and their safety profiles have been fully established (Hellstrand, 2002; Warner and Mitchell, 2004; Pasquier *et al*, 2010). TL-118 drug combination was recently approved by the FDA for an anti-cancer clinical trial (Tiltan Pharma Ltd, 2008, 2012).

The current study aimed to assess the therapeutic potential of TL-118 for CRLM eradication in mice. The therapeutic efficacy was compared with B20-4.1.1 (B20), the human- and

*Correspondence: Dr R Abramovitch; E-mail: rinat@hadassah.org.il

⁴These authors contributed equally to this work.

Revised 26 June 2012; accepted 26 June 2012; published online 17 July 2012

mouse-VEGF-binding monoclonal antibody (Liang *et al*, 2006; Singh *et al*, 2010), and the mTOR pathway inhibitor rapamycin (RAPA) (Guba *et al*, 2002), two well established anti-angiogenic agents. B20-4.1.1 is an anti-VEGF antibody, which has previously been used as a surrogate for preclinical modelling of bevacizumab activity, because it has affinity toward VEGF similar to bevacizumab, yet effectively blocks both the human and murine ligands (Liang *et al*, 2006; Singh *et al*, 2010). RAPA, besides of its immunosuppressive effect, has been shown to exert antiproliferative and anti-angiogenic effects both *in vitro* and *in vivo* (Guba *et al*, 2002; Gridelli *et al*, 2008).

Hemodynamic response imaging (HRI) is a functional MRI (fMRI) method combined with brief exposure to hypercapnic and hyperoxic challenges that was previously demonstrated, enabling monitoring changes in liver perfusion and hemodynamics without the need for contrast agents (Barash *et al*, 2007). The HRI method has been proved sensitive to changes in vessel density, blood flow, oxygen delivery and vessel maturation during tumour progression and anti-angiogenic therapies (Abramovitch *et al*, 1999, 2004). An additional aim of the current research was to evaluate if this method presents a feasible means of determining hemodynamic biomarker profiles indicative of response to anti-angiogenic therapies in CRLM.

In the present study, TL-118 treatment demonstrated a remarkable therapeutic effect with increased animal survival, reduced tumour perfusion and progression as compared with B20 and RAPA, in a well-established mouse model of CRLM. Liver-HRI maps revealed significant attenuated hepatic blood flow during the early phase of TL-118 therapy, illustrating the utility of this technology as indicative biomarker for treatment response. The underlying mechanism for the improved therapeutic effect was associated with hepatic perfusion attenuation resulting from reduced nitric-oxide (NO) serum levels. Previous studies have described the direct impact of decreased NO concentrations on tumour growth, because of its critical role in tumour blood vessel development (Fukumura *et al*, 2001; Camp *et al*, 2006). Conversely, a number of works have suggested that administration of vasopressors (including NO inhibitors), together with anti-tumour drugs, can induce concomitant blood shunting and improve drug delivery to the tumour (Hemingway *et al*, 1992; Shankar *et al*, 1999), regardless of the role of NO in the angiogenic process. Thus, we further reduced the systemic hepatic perfusion during the initial treatment phase of both TL-118 and B20 by adding NO inhibitor and proved that it has a synergistic effect, resulting in improved outcome of both treatments.

MATERIALS AND METHODS

Mouse model of CRLM

All experiments were performed in accordance with the guidelines and approval of the Animal Care and Use Committee of the Hebrew University, which holds the NIH approval (OPRR-A01-5011). CT-26-murine colorectal adenocarcinoma cells (10^4 cells in $300 \mu\text{l}$ per mouse) were intrasplenically injected to 7–8 week-old, anaesthetised male CB6F1 mice (Harlan, Ein-Kerem, Israel) as previously described (Edrei *et al*, 2011). In this model, 1–5 hepatic nodules per mouse were detected by MRI, 13–17 days after cell inoculation.

Table 1 TL-118 treatment composition and regimen

	Sunday	Monday	Tuesday	Wednesday	Thursday	Friday
Cyclophosphamide (mg kg^{-1})	60			60		
Diclofenac (mg kg^{-1})	30			30		
Sulfasalazine (mg kg^{-1})	50	150	150	50	150	150
Cimetidine (mg kg^{-1})		60	60		60	60

TL-118

The TL-118 drug combination (Tiltan Pharma Ltd., Jerusalem, Israel) (Ben-Sasson, 2008) is composed of a low-dose cytotoxic agent (cyclophosphamide) (Browder *et al*, 2000), a COX1/2 inhibitor (diclofenac) (Grunewald *et al*, 2006), a H2 receptor antagonist (cimetidine) (Natori *et al*, 2005; Kubecova *et al*, 2011) and an NF- κ B inhibitor (sulfasalazine) (Weber *et al*, 2000; Chung *et al*, 2009; Li *et al*, 2009). The TL components were intraperitoneally administered according to the schedule outlined in Table 1. The optimisation process included examination of the effect of different concentrations on mice weight as a measure of toxicity. In the optimisation process, we found that in the cytotoxic days (Sunday and Wednesday) it is necessary to reduce the dose of sulfasalazine in order to prevent animal weight loss. The optimal doses determined in mice have been translated into doses suitable for human, based on a body surface area, and were found to be within the acceptable range for clinical use. Moreover, in a phase I clinical trial it was found that this combined protocol composition is well tolerated by the patients.

Treatments

All the treatments started only after CRLM detection by MRI (day 14 ± 2). Mice presenting similar CLRM burden, as detected by MRI, were randomly assigned to the different treatment groups (Figure 1C and D). The CRLM-bearing mice were treated, via intraperitoneal (IP) injection, with TL-118 at a volume of 8 ml kg^{-1} per day (days 1–6 according to the treatment protocol, as described in Table 1, $n = 16$), B20 anti-mouse VEGF antibody (Genentech Inc., San Francisco, CA, USA) at a dose of 5 mg kg^{-1} three times per week ($n = 10$), RAPA (Fermentek Ltd, Jerusalem, Israel) at a dose of 2 mg kg^{-1} per day ($n = 8$) or an inert vehicle (control group) at a volume of 8 ml kg^{-1} per day ($n = 14$). The treatments were continued until the tumour load reached ethical restrictions ($1 \pm 0.2 \text{ mm}^3$) or up to 2 months in mice, which demonstrated tumour disappearance. Additional groups of naive mice (without tumours) were treated with TL-118 ($n = 10$) or B20 ($n = 5$) with the same protocol regimen as described above for 21 days. Additional groups of CRLM-bearing mice were implanted subcutaneously with micro-osmotic pump (Alzet model 1002; DURECT Corporation, Cupertino, CA, USA) containing NO inhibitor (N-Nitro-L-arginine methyl ester hydrochloride (L-NAME); Sigma Aldrich, St Louis, MO, USA) at a dose of 20 mg kg^{-1} per day for 2 weeks from the day of tumour detection and the treatment was combined with either TL-118 ($n = 6$), B20 ($n = 6$) or inert vehicle ($n = 6$) at the standard regimen for 14 days (due to the osmotic pump limitations).

Imaging

Anatomical and fMRI scans were performed on a horizontal 4.7T Biospec spectrometer (Bruker Medical, Ettlingen, Germany) with a 3.5-cm birdcage coil.

Anatomical MRI Mice were anaesthetised with isoflurane (Nicholas Piramal India Ltd, London, UK; 2% in a mixture of 30:70 $\text{O}_2:\text{N}_2\text{O}$) and placed in a supine position. Tumours were assessed twice a week using T_2 -weighted (T_2W) fast spin-echo

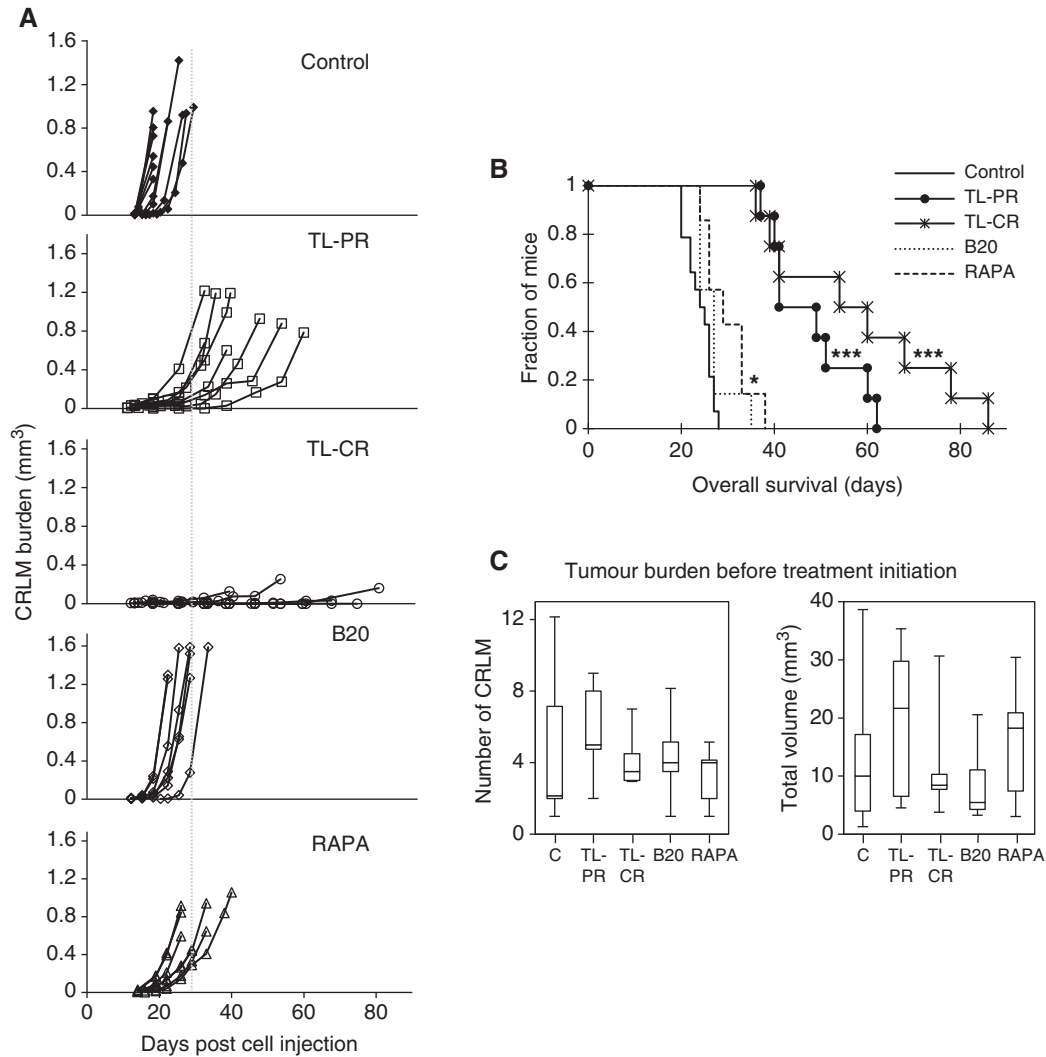


Figure 1 The effects of TL, B20 and RAPA treatments on tumour growth and mouse survival in a mouse model of CRLM. **(A)** The total metastatic volume (mm³) for each individual mouse, as measured from T₂W MRI as a function of time post cell injection (days) in control- ($n = 14$), TL-118- (TL-PR, $n = 8$; TL-CR, $n = 8$), B20- ($n = 10$) and RAPA- ($n = 8$) treated mice. The dashed line marks the maximal survival day of the control-treated group. **(B)** Kaplan–Meier survival analysis for each of the treated groups. * $P = 0.006$ and *** $P < 0.0001$ compared with control. It should be taken into account that the longer the survival, the higher is the risk for tumour-unrelated death due to the repeated pentobarbital anaesthesia for imaging purposes (80%). **(C)** Tumour load prior to treatment initiation. Box and Whiskers plots of the mean number of metastatic foci per mouse (left) and the mean tumour burden (mm³) per mouse (right), as measured from T₂W MRI prior to therapy initiation, for the mice randomly assigned to each treatment group. The differences between the groups were insignificant.

images (repetition time = 2000 ms; echo time = 37 ms; in plane resolution = 117 μ m; and slice thickness = 1 mm).

Hemodynamic response imaging Hemodynamic changes were evaluated by HRI on pentobarbital anaesthetised mice (CTS group, Hod-Hasharon, Israel; 30 mg kg⁻¹, IP) once a week during the treatment period. Images were acquired using T₂*-weighted gradient echo images (repetition time = 147 ms; echo time = 10 ms; field of view = 3 cm; in plane resolution = 117 μ m; slice thickness = 1 mm; two averages; and 37 s per image), under normoxic, hyperoxic and hypercapnic conditions. The hypercapnic- and hyperoxic-reactivity maps are given as the percentage change of signal intensity (ΔS) (Barash *et al*, 2007).

ΔR_2^* maps Multi-gradient echo sequence was used to quantify the transverse relaxation rate R_2^* (repetition time = 200 ms; initial echo time = 5 ms; echo time spacing = 5 ms; five echo times; flip angle $\alpha = 40^\circ$; two averages; and total imaging time ~ 3.5 min).

R_2^* maps were acquired under either normoxic, hypercapnic or hyperoxic conditions.

Image analysis and statistics

The number of tumours per liver and their volumes were assessed from the T₂W images using Analyze-7.0 (BIR, Mayo Clinic, Rochester, MN, USA). Survival curves were constructed according to the Kaplan–Meier method and statistical significance was determined by the log-rank test. The HRI maps and ΔR_2^* maps were generated as reported previously (Barash *et al*, 2007; Barash *et al*, 2008; Edrei *et al*, 2011) using interactive data language (ITT Visual Information Solutions, Boulder, CO, USA). For healthy mice, the selected regions of interest (ROI) covered the entire liver. For CRLM-bearing mice, tumour ROI included the entire lesion and liver ROI included representative liver tissue distant from the detected tumours, as defined by analysis of the T₂W images using the Analyze-7.0 software. Tumours that reached

a size of 0.15 mm^3 are considered as progressed tumours. Mean ΔS values of these ROIs were calculated by including only pixels with a statistical threshold of $P < 0.05$ (active pixels), as calculated by one-sided Mann–Whitney U -test. The percentage of active pixels was calculated for each gas challenge. All of these values are expressed as means and 95% confidence intervals (CIs). The difference between groups was analysed by two-sided Mann–Whitney U -test. Statistical analyses were performed with the Instat Biostatistics software (GraphPad Software Inc., San Diego, CA, USA). A P -value of < 0.05 was considered statistically significant.

Histology and immunostaining

Mice were killed after the final MRI scans and their livers were fixed in 4% formaldehyde. Several samples of CRLM and liver tissues were taken from each mouse and further embedded in paraffin. These liver segments were cut into $4 \mu\text{m}$ slices and stained with hematoxylin and eosin (H&E) or subjected to immunohistochemical analyses. Quantification of necrosis was performed using the Ariol image analysis system (Genetix, San Jose, CA, USA) by scanning H&E-stained slides (12 lesions per group) with an automated scanning microscope. BrdU staining was performed using a Cell Proliferation Kit (GE Healthcare, Amersham, Buckinghamshire, UK), according to the manufacturer's protocol. Apoptosis was assessed through the terminal deoxynucleotidyl transferase-mediated deoxyuridine triphosphate nick-end labelling (TUNEL) assay (Cell Death Detection Kit POD, Roche Diagnostics Corp., Mannheim, Germany), according to the manufacturer's protocol. Nuclei were stained with DAPI, tumour blood vessels were detected using anti-PECAM-1 antibodies (CD31; Biocare Medical, Concord, CA, USA), mature tumour blood vessels were detected using α -smooth muscle actin (α -SMA) antibodies (dilution 1 : 300; Sigma Chemical Co., St Louis, MO, USA) and bile ducts within CRLMs were detected using a rat anti-A6 antibody (kindly provided by Valentina Factor). All the immunostainings were evaluated in 10 randomly selected high-power microscopic fields of viable tumour regions only (magnification $\times 400$), and the mean value and 95% CIs of positive cells or vessels were calculated. The difference between groups was analysed by two-sided Mann–Whitney U -test.

Nitric oxide assay

Blood samples ($300 \mu\text{l}$) were collected from mice tail veins on the specified days, in the presence of heparin, and the plasma was further separated by centrifugation (1200 r.p.m. for 10 min). Plasma NO concentrations were determined by measuring nitrate and nitrite using a nitrate/nitrite colorimetric assay kit (Cayman Chemical, Ann Arbor, MI, USA), according to the manufacturer's instructions.

RESULTS

Impact of anti-angiogenic therapies on tumour progression and mouse survival

MRI-based assessment of the impact of the three anti-angiogenic therapies on CRLM progression (Figure 1A) demonstrated exponential tumour-growth kinetics in control-treated mice, whereas delayed progression with a slight influence on overall animal survival was observed for both B20- and RAPA-treated mice (Figure 1A and B). Only TL-118-treated mice showed significant tumour-growth delay, which could be categorised as either partial response (PR) or complete response (CR). In this animal model, we considered tumours that reached a size of 0.15 mm^3 as progressed tumours. In TL-PR mice ($n = 8$), an approximate 15-day period of delay in tumour progression was observed, which eventually burst into exponential growth.

Furthermore, tumour progression was fully blocked in the TL-CR group ($n = 8$), and in half of the cases, tumour regression with full disappearance of the tumours was observed (see an example in Supplementary Figure 1). Moreover, TL therapy prolonged mean animal survival of CRLM-bearing mice by twofold in the PR group and threefold in the CR group, when compared with control-treated mice (Figure 1B; $P < 0.0005$). It should be taken into account that in the TL-CR group, 80% of the mice died due to the pentobarbital repeated anaesthesia unrelated to tumour burden.

Impact of anti-angiogenic therapies on tumour morphology

Detailed histological examination of control-treated CRLMs revealed distinct tumour borders, high cell proliferation and a low percentage of apoptotic cells (Figure 2A, F and G). In contrast, TL therapy induced massive necrosis (Figure 2B and E; $P < 0.0005$), significantly inhibited cell proliferation, particularly at the tumour centre (Figure 2F; 77% reduction, $P < 0.0005$), and induced a 20-fold elevation in the number of apoptotic cells (Figure 2G; $P < 0.0005$). In addition, tumour borders appeared indistinct with hepatocytes infiltration in the TL-PR mice (Figure 2B) and appearance of enlarged bile ducts integrated within tumour tissue and vessel cooption were detected (Supplementary Figure 2A–C). Tumours of both B20- and RAPA-treated mice, retained distinct borders and had only few necrotic regions (Figure 2C–E). Although these therapies inhibited cell proliferation (Figure 2F; 35% and 30% reduction, respectively, $P < 0.05$), it also significantly reduced the number of apoptotic cells (Figure 2G; $P < 0.0005$ and < 0.05 , respectively). Finally, although no metastases could be detected by MRI in the TL-CR mice during the study period, histological examination of liver specimens performed subsequent to experiment completion, 3 month after cell inoculation, revealed residual tumour cells in these livers (Supplementary Figure 2D–I).

Impact of anti-angiogenic therapies on tumour vascularisation

Immunohistological analysis revealed significantly reduced CD31^+ intratumoural vessel density in all the treated tumours, with the most prominent decrease observed in the TL-PR subgroup (Figure 3G; ninefold, $P < 0.005$). When analysing the vessel maturation status, most of the vessels were α -SMA⁺ (Figure 3). Morphological changes in vessel integrity were observed in TL-PR mice, where vessels appeared collapsed (Figure 3B). Moreover, numerous blood vessels in B20-treated and RAPA-treated CRLM were extremely widened and α -SMA⁺ (Figure 3C and D). The HRI-based assessment of the vascular and hemodynamic changes occurring in the treated tumours demonstrated a significant decrease in tumour-HRI values of TL- and RAPA-treated mice (Figure 3E and F; $P < 0.005$ and < 0.05 , respectively). The percent reduction in tumour-HRI values was in good correlation with treatment success as measured by the delay in tumour-growth progression and mice survival (Figure 1).

Anti-angiogenic therapies affect liver perfusion

During the early stages of TL treatment, HRI values of the entire liver parenchyma, in CRLM-bearing mice, were significantly lower compared with control-treated mice (Figure 4A and E; $P < 0.0005$) with the most prominent decrease observed in the TL-CR subgroup. Additionally, the liver-HRI values of RAPA- and B20-treated mice were also reduced significantly (Figure 4E; $P < 0.0005$). As seen with CRLM-bearing mice that were treated with anti-angiogenic therapies, a significant decrease in liver reactivity was also observed in naive treated mice, already after 10 days of treatment. The reduced values remained low for at least

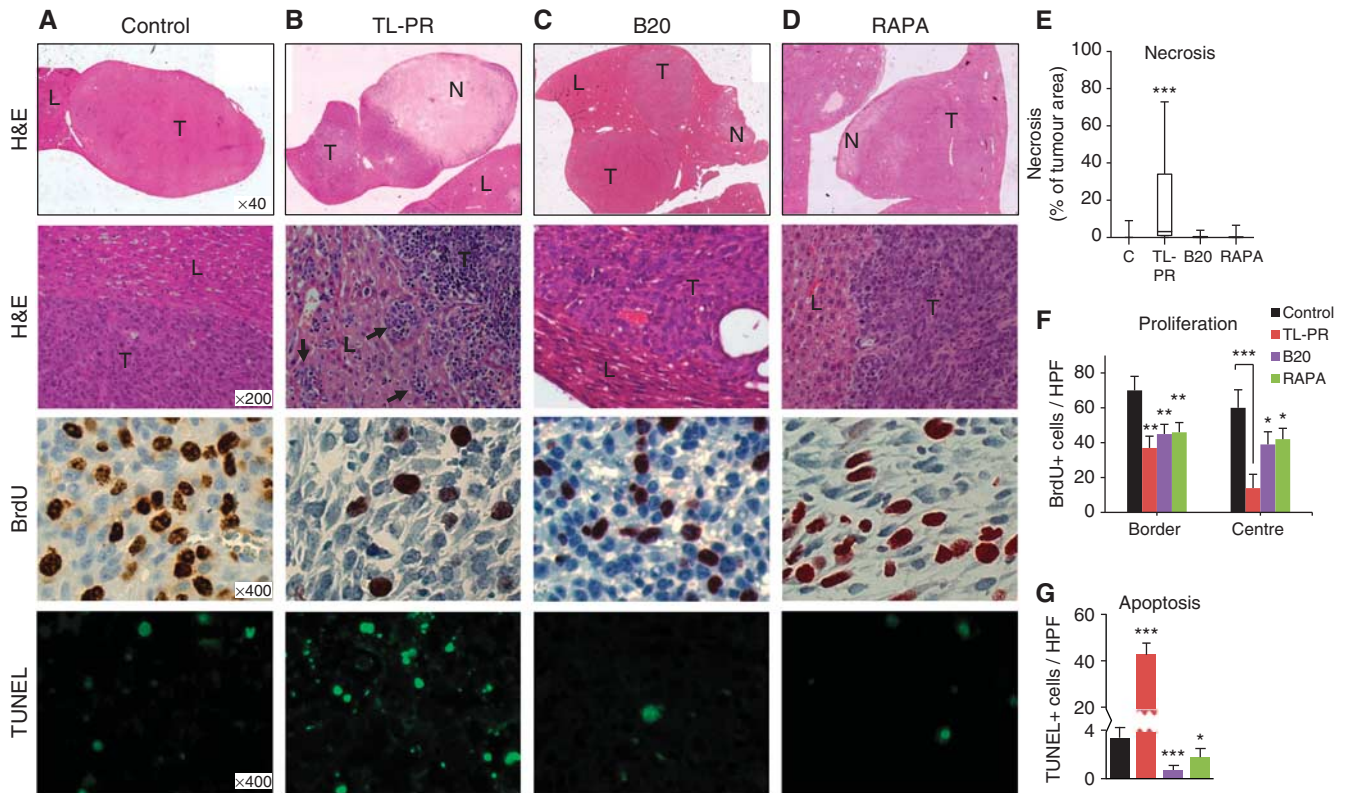


Figure 2 Effects of anti-angiogenic therapies on CRLM morphology. Representative histological sections of control- (A), TL-PR- (B), B20- (C) and RAPA- (D) treated mice. Slides were stained with H&E (first and second rows), BrdU (third row) and TUNEL (fourth row) to allow for respective quantitative assessment of necrosis (E, box-and-whiskers plot; $n = 15$ tumours per group), tumour cell proliferation (F, BrdU-positive cells; calculated from 10 fields of each of the nine tumours analysed per treatment group) and apoptosis (G, TUNEL-positive cells; $n = 10$ high-power microscopic field (HPF) per mouse; four mice per group). Original magnification is indicated on the left image of each row. $*P < 0.05$, $**P < 0.005$ and $***P < 0.0005$. The histological sections were taken at the end of the experiments when the tumour load per mouse reached ethical limits ($1 \pm 0.2 \text{ mm}^3$). Abbreviations: T = tumour tissue; L = liver tissue; and N = necrotic areas.

1 month (Figure 4B–D and F; $P < 0.0005$), demonstrating a CRLM-independent effect of TL or B20 therapies on liver perfusion.

The decrease of liver-HRI reactivity was proven previously to be associated with reduced liver perfusion (Barash *et al*, 2008). Because ΔR_2 maps reflect changes in tissue oxygenation, with no effect from flow rate (Howe *et al*, 2001), we compared HRI and ΔR_2^+ maps of naive- vs TL-treated livers. Although the liver-HRI maps were significantly attenuated in the treated mice, the corresponding ΔR_2 maps were highly similar (Supplementary Figure 3). Thus, we concluded that both TL and B20 treatments led to reduced hepatic blood flow. In line with these findings, both treatments were found to significantly decrease serum NO levels when compared with naive untreated mice (Figure 4G; $P < 0.005$). Thus, we hypothesised that NO levels during early treatment stages inversely correlated with therapeutic potential.

Reduced systemic NO level improves anti-angiogenic therapy

In order to verify the suspected association between the reduced serum NO levels and the anti-angiogenic therapeutic outcome, we evaluated the synergistic effect of NO inhibitor on both TL and B20 therapies. Mice with clearly identifiable CRLM were treated with L-NAME (during the first 2 weeks due to the osmotic pump limitations) combined with the standard TL or B20 regimen. Liver metastases were fully eradicated in the TL + L-NAME-treated mice (Figure 4H, top), whereas in the B20-treated mice, only moderate improvement was observed; yet, in two of these mice the tumours were completely eliminated (Figure 4H, bottom). Treatment with

L-NAME alone had a subtle effect on tumour progression (data not shown). These results suggest that reducing blood flow to the liver at early stages of the anti-angiogenic treatment is crucial for achieving maximal anti-tumour effects.

DISCUSSION

The considerably poor prognosis of patients presenting CRLMs and the insufficient efficacy of available treatment options have called for the development of alternative curative strategies. Although, VEGF-targeted therapies have shown some promising results, new anti-angiogenic approaches are still required to fully curb distal growth of tumour mass. By careful selection of mechanistically unrelated agents, each targeting a different aspect of angiogenesis, the TL-118 cocktail offers a multi-faceted mean of intervening with the complex angiogenic process by providing a synergistic composition.

The comparative analysis of TL, B20 and RAPA treatment outcomes demonstrated an unequivocal advantage to TL therapy, as demonstrated through the significant increase in mean animal survival, the reduced vessel density and tumour perfusion, increased apoptosis and necrosis and decreased proliferation within the tumour core when compared with control mice. Although some of these phenomena were also observed in B20- and RAPA-treated mice, the therapeutic potential of the TL-118 treatment was significantly superior. More specifically, in cases of CR, TL tripled the mean mouse-survival period and completely abolished MRI-detectable metastatic foci, resulting in

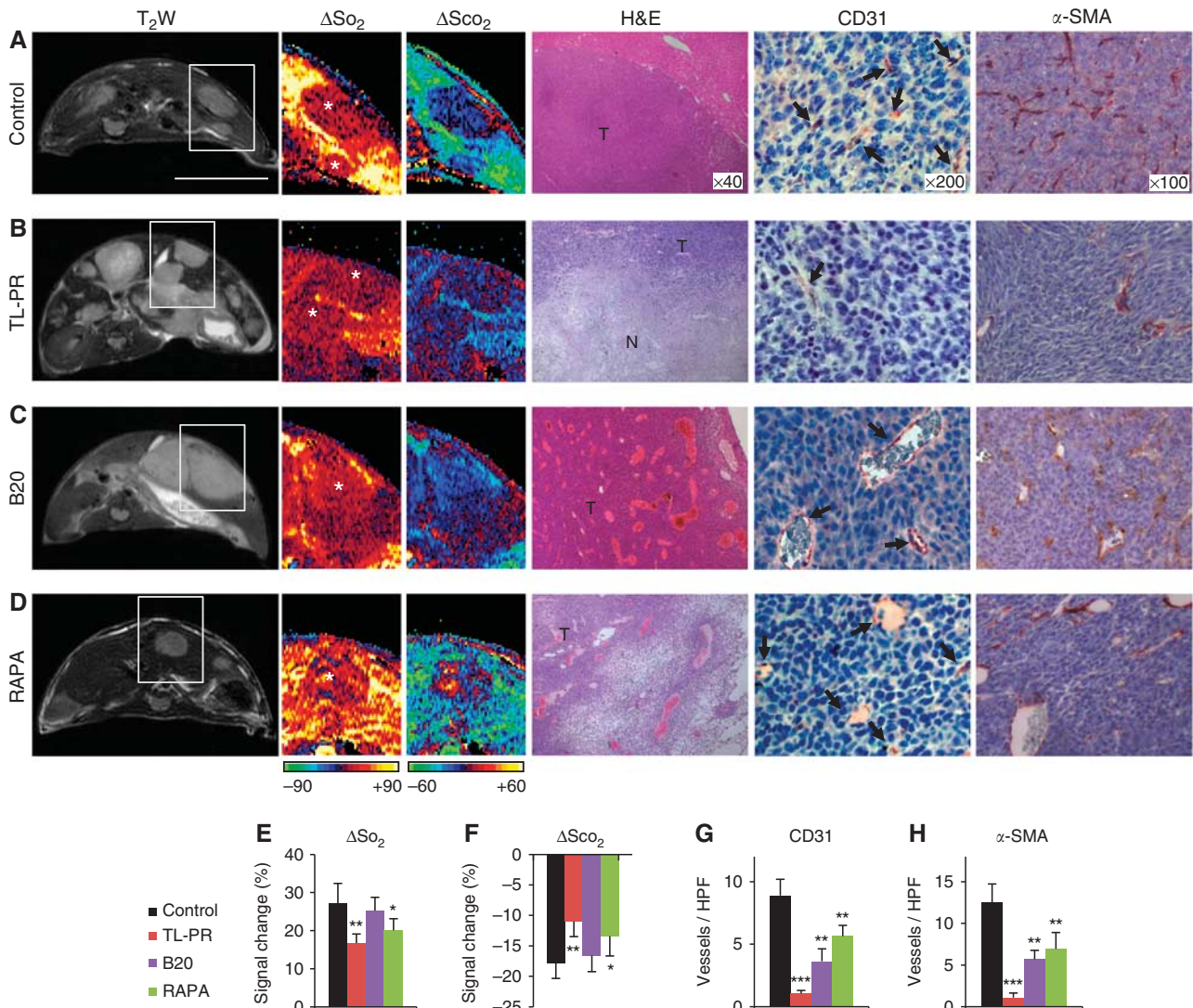


Figure 3 Effects of anti-angiogenic therapies on CRLM vasculature and perfusion. Representatives axial T₂W images (first column from left, Bar = 1 cm), and the corresponding enlarged (× 2) HRI maps (second and third columns) of the indicated tumour region (white box, tumours are marked by white asterisks). Representative histological slides were stained with H&E (fourth column), with the endothelial cell marker CD31 (fifth column; arrows point to vessels) and α-SMA (sixth column) of control- (A), TL-PR- (B), B20- (C) and RAPA- (D) treated mice. In TL-PR mice, vessels appeared collapsed (B), whereas in B20- and RAPA-treated mice, numerous blood vessels were extremely widened (C, D). Mean ΔS₀₂ (E) and mean ΔS₀₂ (F) values with 95% CIs were calculated from 13 tumours per treatment group during tumour progression. (G) Quantification of CD31-positive vessels per HPF; (H) Quantification of α-SMA-positive vessels per HPF. The quantitative data (G, H) were calculated from 10 fields for each of the nine tumours analysed per treatment group. Original histological magnification is indicated on image A of each row. **P < 0.005 and ***P < 0.0005. The histological sections were taken at the end of the experiments when the tumour load per mouse reached ethical limits (1 ± 0.2 mm³). Abbreviations: T = tumour tissue and N = necrotic areas.

complete remission. Moreover, in the TL-CR group most of the mice died due to the pentobarbital repeated anaesthesia unrelated to tumour burden.

Numerous studies on xenograft tumour models have demonstrated the marked ability of VEGF-blocking agents to suppress tumour progression, with occasional tumour regression (Kim *et al*, 1993; Rowe *et al*, 2000a, 2000b; Huang *et al*, 2003). However, none of these agents have successfully cured animals, even when combined with other therapies. When considering the relatively advanced stage of metastases in the present model, the remarkable therapeutic capacity of TL-based therapy is further highlighted. This disparity in therapeutic impact is most likely rooted in the nature of the multitasking TL-118 cocktail, better suited to combat the multi-faceted angiogenic process. It has been suggested that the effective therapeutic window for anti-VEGF therapy precedes vessel maturation (Benjamin *et al*, 1999). Analysis of the CRLM

vessel-maturation status demonstrated a high degree of α-SMA-positive intratumoural vessels both before (data not shown) and during B20 and RAPA therapies. These findings elucidate the origin of B20 and RAPA therapeutic failure, while strengthening the powerful potential of TL treatment at advanced disease stages.

As demonstrated by HRI of naive treated mice, both TL and B20 therapies affect liver perfusion independent of tumour presence. Losser *et al* (2010) reported significant hepatic artery vasoconstriction and subsequent reduction in arterial flow velocity upon NOS inhibition in healthy rabbits. Indeed, systemic downregulation of NO serum concentrations correlated with TL- and B20-stimulated hemodynamic responses and is suggested to form the mechanistic basis of reduced liver perfusion.

Nitric-oxide is known to mediate vasodilation and rapidly induce alterations in blood flow (Moncada *et al*, 1991). In contrast, NO-synthase inhibition induces sinusoidal vessel constriction,

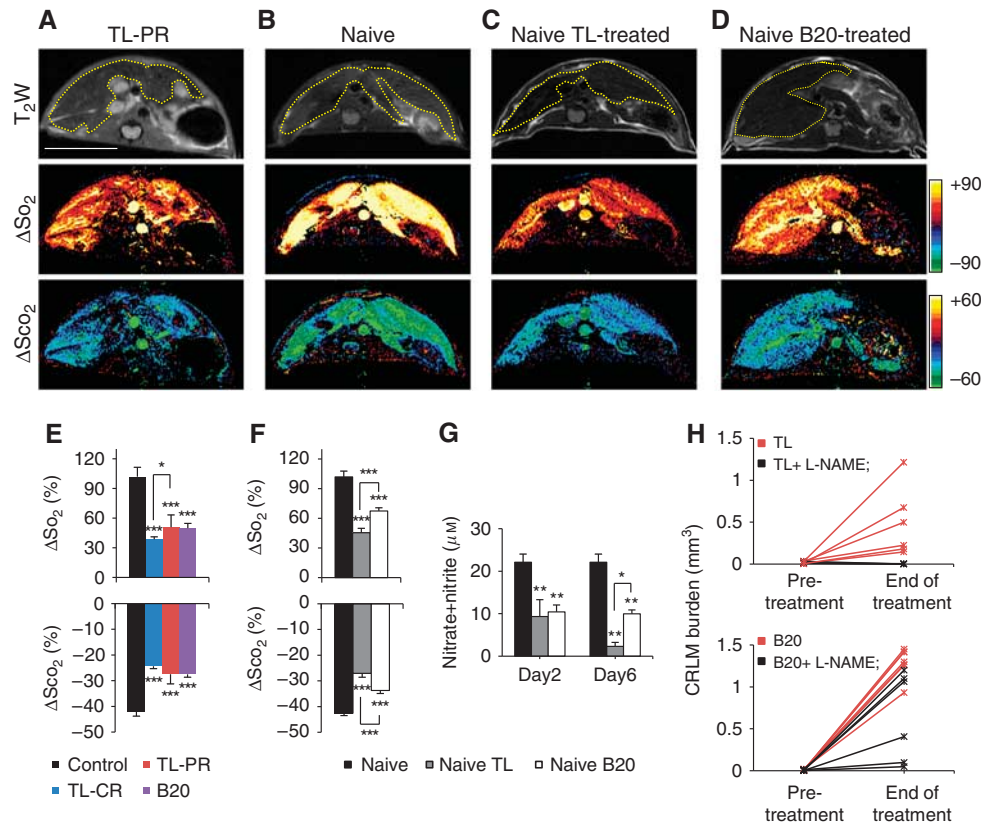


Figure 4 Hepatic perfusion attenuation during TL and B20 treatments. (**A–D**) Representative axial T₂W MR images (top row) and the corresponding HRI maps of ΔSO_2 (middle row) and ΔSCO_2 (bottom row) obtained from a TL-PR-treated (**A**), naive (**B**), naive TL-treated (**C**) and naive B20-treated (**D**) mice. Liver borders are marked in yellow, Bar = 1 cm; (**E**) Mean hepatic ΔSO_2 and ΔSCO_2 values with 95% CIs of control- ($n = 14$ mice), TL-PR- ($n = 8$ mice), TL-CR- ($n = 8$ mice) and B20- ($n = 6$) treated CRLM-bearing mice. (**F**) Mean hepatic ΔSO_2 and ΔSCO_2 values with 95% CIs of naive ($n = 10$ mice), naive TL-treated ($n = 10$ mice) and naive B20-treated ($n = 5$ mice) mice. (**G**) Nitrate plus nitrite serum levels with 95% CIs were analysed from blood samples obtained before ($n = 10$ mice) and during TL and B20 treatments of naive mice ($n = 5$ mice per time point). (**H**) Systemic NO inhibition improves TL and B20 therapies. The total metastatic volume for each individual mouse before and at the end of treatment in TL- (top; TL-PR, $n = 8$ and TL + L-NAME, $n = 5$) and B20-treated (bottom; B20, $n = 10$ and B20 + L-NAME, $n = 6$) mice. * $P < 0.05$, ** $P < 0.005$ and *** $P < 0.0005$.

which decreases flow and results in hypertension. Some studies have suggested that vasopressor administration (including NO inhibitor) may lead to blood shunting into the tumour concomitantly with improved drug delivery (Hemingway *et al*, 1992; Shankar *et al*, 1999). Conversely, a number of works have described the direct impact of decreased NO concentrations on tumour growth, because of its critical role in tumour blood vessel development. They demonstrated that VEGF-mediated angiogenesis relies, at least in part, on the downstream effects of NO (Fukumura *et al*, 2001; Camp *et al*, 2006). Nevertheless, treatment with NO inhibitor combined with TL-118 in a subcutaneous tumour model failed to induce any additive effect compared with TL-118 alone (data not shown). The current findings suggest that although the reduced NO levels affect the systemic blood flow, only liver metastases were influenced from this strategy. Therefore, we suggest that reduced blood flow to the liver at early stages of the anti-angiogenic treatment is crucial for achieving maximal anti-tumour effects. The combination of NO inhibitor and B20 had only a moderate impact on tumour growth compared with the combination with TL. Because the reduction of the systemic NO level by TL was greater than that obtained by B20, we assume that an additional increase of the NO inhibitor dosage with B20 therapy may improve the therapeutic outcome.

Both B20 and RAPA treatment yielded similar morphological profiles of reduced vascularity with widened vessels and inhibition of cell proliferation, suggesting that both treatments act via the anti-angiogenic and anti-proliferative pathways, as previously

reported (Wang *et al*, 2009; Yang *et al*, 2010). Interestingly, fewer apoptotic cells were detected in the B20-treated group, when compared with control-treated mice. These results may explain the modest therapeutic effect of B20 compared with RAPA. Similar enhancement of vessel diameter and maturation was recently described following bevacizumab therapy of human colorectal adenocarcinoma liver metastases (Weisshardt *et al*, 2011). The increased vessel diameter and maturation following B20 therapy may contribute to improved therapeutic potency when combined with either radiation or chemotherapy, supporting the vessel normalisation mechanism (Jain, 2005).

Study limitations include the use of B20 (Liang *et al*, 2006), which may have contributed to the relatively mild response observed, when compared with those reported in the clinics. Although bevacizumab has been approved for the treatment of metastatic colorectal cancer in combination with the standard chemotherapy (Hurwitz *et al*, 2004; Kabbinavar *et al*, 2005), the present study considered the stand-alone efficacy of B20.

In the present study, TL displayed a remarkable therapeutic effect on CRLM-bearing mice, even when treatment was initiated at advanced metastatic stages, where the vasculature was highly covered with pericytes. The application of the HRI technique provided critical evidence regarding the mechanisms underlying the improved anti-tumorigenic effect of TL, the reduced hepatic perfusion. Indeed, the reduced hepatic perfusion was proven as essential for therapeutic success because the addition of the NO inhibitor during the initial treatment phase of both TL and B20

improved treatment outcome dramatically. Furthermore, HRI has been proven to be a sensitive and beneficial non-invasive tool for monitoring responses to anti-angiogenic therapies.

ACKNOWLEDGEMENTS

We thank Genentech for B20-4.1.1 supply, Tiltan-Pharma for TL-118 supply and Valentina Factor (NIH) for A6-antibodies supply. We thank Mrs Elia Dery for animal experiments

REFERENCES

- Abramovitch R, Dafni H, Smouha E, Benjamin LE, Neeman M (1999) In vivo prediction of vascular susceptibility to vascular susceptibility endothelial growth factor withdrawal: magnetic resonance imaging of C6 rat glioma in nude mice. *Cancer Res* 59(19): 5012–5016
- Abramovitch R, Itzik A, Harel H, Nagler A, Vlodavsky I, Siegal T (2004) Halofuginone inhibits angiogenesis and growth in implanted metastatic rat brain tumor model – an MRI study. *Neoplasia* 6(5): 480–489
- Barash H, Gross E, Edrei Y, Pappo O, Spira G, Vlodavsky I, Galun E, Matot I, Abramovitch R (2008) Functional magnetic resonance imaging monitoring of pathological changes in rodent livers during hyperoxia and hypercapnia. *Hepatology* 48(4): 1232–1241
- Barash H, Gross E, Matot I, Edrei Y, Tsarfaty G, Spira G, Vlodavsky I, Galun E, Abramovitch R (2007) Functional MR imaging during hypercapnia and hyperoxia: noninvasive tool for monitoring changes in liver perfusion and hemodynamics in a rat model. *Radiology* 243(3): 727–735
- Ben-Sasson SA (2008) Anti-cancer therapy comprising an H2-blocker, at least one antiinflammatory agent and a cytotoxic agent. In *US Patent* 7838 513
- Benjamin LE, Golijanin D, Itin A, Pode D, Keshet E (1999) Selective ablation of immature blood vessels in established human tumors follows vascular endothelial growth factor withdrawal. *J Clin Invest* 103(2): 159–165
- Bergers G, Hanahan D (2008) Modes of resistance to anti-angiogenic therapy. *Nat Rev* 8(8): 592–603
- Browder T, Butterfield CE, Kraling BM, Shi B, Marshall B, O'Reilly MS, Folkman J (2000) Antiangiogenic scheduling of chemotherapy improves efficacy against experimental drug-resistant cancer. *Cancer Res* 60(7): 1878–1886
- Camp ER, Yang A, Liu W, Fan F, Somcio R, Hicklin DJ, Ellis LM (2006) Roles of nitric oxide synthase inhibition and vascular endothelial growth factor receptor-2 inhibition on vascular morphology and function in an in vivo model of pancreatic cancer. *Clin Cancer Res* 12(8): 2628–2633
- Chung CH, Lin KT, Chang CH, Peng HC, Huang TF (2009) The integrin $\alpha 2\beta 1$ agonist, aggritin, promotes proliferation and migration of VSMC through NF- κ B translocation and PDGF production. *Br J Pharmacol* 156(5): 846–856
- Edrei Y, Gross E, Corchia N, Tsarfaty G, Galun E, Pappo O, Abramovitch R (2011) Vascular profile characterization of liver tumors by magnetic resonance imaging using hemodynamic response imaging in mice. *Neoplasia* 13(3): 244–253
- Folkman J (1990) What is the evidence that tumors are angiogenesis dependent? *J Natl Cancer Inst* 82(1): 4–6
- Fukumura D, Gohongi T, Kadambi A, Izumi Y, Ang J, Yun CO, Buerk DG, Huang PL, Jain RK (2001) Predominant role of endothelial nitric oxide synthase in vascular endothelial growth factor-induced angiogenesis and vascular permeability. *Proc Natl Acad Sci USA* 98(5): 2604–2609
- Gridelli C, Maione P, Rossi A (2008) The potential role of mTOR inhibitors in non-small cell lung cancer. *Oncologist* 13(2): 139–147
- Grunewald M, Avraham I, Dor Y, Bachar-Lustig E, Itin A, Jung S, Chimenti S, Landsman L, Abramovitch R, Keshet E (2006) VEGF-induced adult neovascularization: recruitment, retention, and role of accessory cells. *Cell* 124(1): 175–189
- Guba M, von Breitenbuch P, Steinbauer M, Koehl G, Flegel S, Hornung M, Bruns CJ, Zuelke C, Farkas S, Anthuber M, Jauch KW, Geissler EK (2002) Rapamycin inhibits primary and metastatic tumor growth by antiangiogenesis: involvement of vascular endothelial growth factor. *Nat Med* 8(2): 128–135
- Hellstrand K (2002) Histamine in cancer immunotherapy: a preclinical background. *Semin Oncol* 29(3 Suppl 7): 35–40
- Hemingway DM, Angerson WJ, Anderson JH, Goldberg JA, McArdle CS, Cooke TG (1992) Monitoring blood flow to colorectal liver metastases using laser Doppler flowmetry: the effect of angiotensin II. *Br J Cancer* 66(5): 958–960
- Howe FA, Robinson SP, McIntyre DJ, Stubbs M, Griffiths JR (2001) Issues in flow and oxygenation dependent contrast (FLOOD) imaging of tumours. *NMR Biomed* 14(7–8): 497–506
- Huang J, Frischer JS, Serur A, Kadenhe A, Yokoi A, McCrudden KW, New T, O'Toole K, Zabski S, Rudge JS, Holash J, Yancopoulos GD, Yamashiro DJ, Kandel JJ (2003) Regression of established tumors and metastases by potent vascular endothelial growth factor blockade. *Proc Natl Acad Sci USA* 100(13): 7785–7790
- Hurwitz H, Fehrenbacher L, Novotny W, Cartwright T, Hainsworth J, Heim W, Berlin J, Baron A, Griffing S, Holmgren E, Ferrara N, Fyfe G, Rogers B, Ross R, Kabbinavar F (2004) Bevacizumab plus irinotecan, fluorouracil, and leucovorin for metastatic colorectal cancer. *N Eng J Med* 350(23): 2335–2342
- Jain RK (2005) Normalization of tumor vasculature: an emerging concept in antiangiogenic therapy. *Science* 307(5706): 58–62
- Kabbinavar FF, Hambleton J, Mass RD, Hurwitz HI, Bergsland E, Sarkar S (2005) Combined analysis of efficacy: the addition of bevacizumab to fluorouracil/leucovorin improves survival for patients with metastatic colorectal cancer. *J Clin Oncol* 23(16): 3706–3712
- Kim KJ, Li B, Winer J, Armanini M, Gillett N, Phillips HS, Ferrara N (1993) Inhibition of vascular endothelial growth factor-induced angiogenesis suppresses tumour growth in vivo. *Nature* 362(6423): 841–844
- Kubecova M, Kolostova K, Pinterova D, Kacprzak G, Bobek V (2011) Cimetidine: an anticancer drug? *Eur J Pharm Sci* 42(5): 439–444
- Li B, Li YY, Tsao SW, Cheung AL (2009) Targeting NF- κ B signaling pathway suppresses tumor growth, angiogenesis, and metastasis of human esophageal cancer. *Molecular Cancer Ther* 8(9): 2635–2644
- Liang WC, Wu X, Peale FV, Lee CV, Meng YG, Gutierrez J, Fu L, Malik AK, Gerber HP, Ferrara N, Fuh G (2006) Cross-species vascular endothelial growth factor (VEGF)-blocking antibodies completely inhibit the growth of human tumor xenografts and measure the contribution of stromal VEGF. *J Biol Chem* 281(2): 951–961
- Losser MR, Lenfant F, Payen D (2010) Modification of the hepatic hemodynamic response to acute changes in PaCO₂ by nitric oxide synthase inhibition in rabbits. *Anesth Analg* 110(3): 845–851
- Mayorek N, Naftali-Shani N, Grunewald M (2010) Diclofenac inhibits tumor growth in a murine model of pancreatic cancer by modulation of VEGF levels and arginase activity. *PLoS One* 5(9): e12715
- McLoughlin JM, Jensen EH, Malafa M (2006) Resection of colorectal liver metastases: current perspectives. *Cancer Control* 13(1): 32–41
- Meyers MO, Watson JC (2003) Angiogenesis and hepatic colorectal metastases. *Surg Oncol Clin N Am* 12(1): 151–163
- Miller KD, Sweeney CJ, Sledge Jr GW (2005) Can tumor angiogenesis be inhibited without resistance? *Exs* 94: 95–112
- Moncada S, Palmer RM, Higgs EA (1991) Nitric oxide: physiology, pathophysiology, and pharmacology. *Pharmacol Rev* 43(2): 109–142
- Natori T, Sata M, Nagai R, Makuuchi M (2005) Cimetidine inhibits angiogenesis and suppresses tumor growth. *Biomed Pharmacother* 59(1–2): 56–60
- Pasquier E, Kavallaris M, Andre N (2010) Metronomic chemotherapy: new rationale for new directions. *Nat Rev Clin Oncol* 7(8): 455–465
- Rowe DH, Huang J, Kayton ML, Thompson R, Troxel A, O'Toole KM, Yamashiro D, Stolar CJ, Kandel JJ (2000a) Anti-VEGF antibody suppresses primary tumor growth and metastasis in an experimental model of Wilms' tumor. *J Pediatr Surg* 35(1): 30–32; discussion 32–33

- Rowe DH, Huang J, Li J, Manley C, O'Toole KM, Stolar CJ, Yamashiro DJ, Kandel JJ (2000b) Suppression of primary tumor growth in a mouse model of human neuroblastoma. *J Pediatr Surg* 35(6): 977–981
- Shankar A, Loizidou M, Burnstock G, Taylor I (1999) Noradrenaline improves the tumour to normal blood flow ratio and drug delivery in a model of liver metastases. *Br J Surg* 86(4): 453–457
- Siegel R, Naishadham D, Jemal A (2012) Cancer statistics, 2012. *CA Cancer J Clin* 62(1): 10–29
- Singh M, Lima A, Molina R, Hamilton P, Clermont AC, Devasthali V, Thompson JD, Cheng JH, Bou Reslan H, Ho CC, Cao TC, Lee CV, Nannini MA, Fuh G, Carano RA, Koeppen H, Yu RX, Forrest WF, Plowman GD, Johnson L (2010) Assessing therapeutic responses in Kras mutant cancers using genetically engineered mouse models. *Nat Biotechnol* 28(6): 585–593
- Sorbo J, Jakobsson A, Norrby K (1994) Mast-cell histamine is angiogenic through receptors for histamine1 and histamine2. *Int J Exper Pathol* 75(1): 43–50
- Tiltan Pharma Ltd (2008) *Phase IIB Clinical Trial of Hamsa-1™ in Metastatic Castration Resistant Prostate Cancer (CRPC) (TLH-202)*. <http://clinicaltrials.gov/ct2/show/NCT00684970>
- Tiltan Pharma Ltd (2012) *A Clinical Trial of Anti-Angiogenic Drug Combination TL-118 for Pancreatic Cancer Patients Who Are Starting Gemcitabine Treatment*. <http://clinicaltrials.gov/ct2/show/NCT01509911>
- Wang Z, Zhou J, Fan J, Tan CJ, Qiu SJ, Yu Y, Huang XW, Tang ZY (2009) Sunitinib inhibits the growth and metastatic progression of hepatocellular carcinoma. *J Cancer Res Clin Oncol* 135(5): 715–722
- Warner TD, Mitchell JA (2004) Cyclooxygenases: new forms, new inhibitors, and lessons from the clinic. *Faseb J* 18(7): 790–804
- Warren RS, Yuan H, Matli MR, Gillett NA, Ferrara N (1995) Regulation by vascular endothelial growth factor of human colon cancer tumorigenesis in a mouse model of experimental liver metastasis. *J Clin Invest* 95(4): 1789–1797
- Weber CK, Liptay S, Wirth T, Adler G, Schmid RM (2000) Suppression of NF-kappaB activity by sulfasalazine is mediated by direct inhibition of IkappaB kinases alpha and beta. *Gastroenterology* 119(5): 1209–1218
- Weisshardt P, Trarbach T, Durig J, Paul A, Reis H, Tilki D, Miroschnik I, Ergun S, Klein D (2011) Tumor vessel stabilization and remodeling by anti-angiogenic therapy with bevacizumab. *Histochem Cell Biol* 137(3): 391–401
- Yang H, Jager MJ, Grossniklaus HE (2010) Bevacizumab suppression of establishment of micrometastases in experimental ocular melanoma. *Invest Ophthalmol Vis Sci* 51(6): 2835–2842

This work is published under the standard license to publish agreement. After 12 months the work will become freely available and the license terms will switch to a Creative Commons Attribution-NonCommercial-Share Alike 3.0 Unported License.